

RESEARCH

Open Access



Axial–Flexural Interaction in FRP-Wrapped RC Columns

Hanan Suliman Al-Nimry* and Rabi Amer Al-Rabadi

Abstract

The study reported herein aims at investigating the behavior of medium-scale circular reinforced concrete columns wrapped with fiber reinforced polymer (FRP) sheets under concentric and eccentric axial loads. The experimental program was devised to assess the effects of loading conditions, absence/presence of an FRP jacket as well as the FRP wrapping system. To achieve the study objectives, four column groups were tested under axial compression at 0, 25, 50 and 65 mm loading eccentricities corresponding to eccentricity-to-diameter ratios of 0, 0.13, 0.26 and 0.34, respectively. Specimens in a fifth group were tested in pure bending simulating axial compression at infinite loading eccentricities. Three column subcategories were tested under each of the 5 loading eccentricities: unwrapped; wrapped with one ply of hoop FRP sheets; and wrapped with two FRP plies with fibers oriented at 0 and 90° to the longitudinal column axis thereby providing externally-bonded longitudinal reinforcement and hoop confinement, respectively. Tests confirmed that FRP confinement enhances the axial–flexural column resistance even at large eccentricities that exceed the balanced state of unconfined columns. Although axial column resistance decreased with increasing bending moments, relative enhancements (25–35%) in axial resistance provided by FRP confinement were found to be more significant under eccentric loading than in pure compression. Compared to hoop FRP-confined columns, using additional longitudinal sheets resulted in minor (7–9%) but stable enhancements in axial resistance that were unaffected by the increase in loading eccentricity. The FRP hoop wraps had a minor effect on the flexural resistance of specimens tested in pure bending but managed to double their resistance when combined with the externally-bonded longitudinal FRP sheets. Finally, three stress–strain models of FRP-confined concrete were used in conventional section analysis to assess the axial–flexural interaction in the FRP-jacketed columns. Strength predictions made using the stress–strain model proposed in ACI 440.2R-17 design guidelines did not agree with the test results of the eccentrically-loaded columns and underestimated the moment resistance at a given axial force even when considering higher confinement ratios than those permitted by the guidelines. Strength predictions made using eccentricity-dependent stress–strain models showed better results especially when accounting for the increase in ultimate axial strains under eccentric loading.

Keywords: reinforced concrete, circular columns, FRP wrapping, CFRP, confinement, axial–flexural interaction, toughness, deformation capacity, ductility

1 Introduction

External wrapping using fiber reinforced polymer (FRP) sheets has become a well-established technique that is typically used to retrofit some of the commonly encountered inadequacies of reinforced concrete (RC) columns

in substandard buildings and bridges. The relative ease of implementation of this technique is one of the main reasons for its frequent use in repairing damaged concrete columns or meeting higher load capacity or ductility demands imposed by changes in facility use or even rigorous updates of code provisions. In FRP jacketing unidirectional sheets are usually implemented with the main fibers aligned along the column's hoop direction providing passive confinement to the core concrete. In such case the beneficial effects of the orthotropic sheets,

*Correspondence: hsnimry@just.edu.jo
Department of Civil Engineering, Jordan University of Science and Technology, P.O. Box 3030, Irbid 22110, Jordan
Journal information: ISSN 1976-0485 / eISSN 2234-1315

which exhibit their largest strength along the fiber direction, are subject to the type of applied loading.

Being aware that columns in real structures are expected to experience flexural loading as a result of applied end moments or at least accidental loading eccentricities, researchers have addressed the effects of different loading combinations. A number of recent studies have examined the performance of FRP-confined columns under eccentric axial loading (Parvin and Wang 2001; Li and Hadi 2003; Ghali et al. 2003; Tao et al. 2004; Hadi 2006a, b, 2007, 2009; Yi et al. 2006; El Maaddawy 2009; El Maaddawy et al. 2010; Bisby and Ranger 2010; Fitzwilliam and Bisby 2010; Sadeghian et al. 2010; Hadi and Widiarsa 2012; Csuka and Kollár 2012; Daugevičius et al. 2013; Song et al. 2013; Widiarsa and Hadi 2013; Wu and Jiang 2013; Youcef et al. 2015; Lin and Teng 2016, 2017; Vuggumudi and Alagusundaramoorthy 2018; Yang et al. 2018; Chellapandian and Prakash 2019; Chellapandian et al. 2019a, b; Al-Nimry and Neqresh 2019) showing a limited ability of columns wrapped with unidirectional FRP sheets with the main fibers aligned along the hoop direction to resist eccentric compression.

Bisby and Ranger (2010), Al-Nimry and Neqresh (2019), Chaallal and Shahawy (2000) and Pham et al. (2013) have used stress–strain models derived from concentric loading tests of FRP-confined concrete to develop axial force–bending moment (P – M) interaction diagrams and have reached contradicting conclusions. Chaallal and Shahawy (2000) showed that the experimental moment capacity under a certain axial force is smaller than the theoretical value calculated using a stress–strain model derived from concentrically-loaded tests whereas Bisby and Ranger (2010) and Al-Nimry and Neqresh (2019) arrived at an opposing conclusion, i.e. the theoretical P – M interaction diagrams provide conservative predictions of the actual response. Pham et al. (2013), on the other hand, proved that using such stress–strain models to develop theoretical P – M charts results in values that do not agree well with the experimental results. Pham et al. (2013) confirmed that as the ratio of loading eccentricity to column radius exceeds 0.47 the calculated moment values exceed the test values.

To date, many of the widely used design guidelines for FRP-confined RC columns (CNR 2013; TR 55 2012; ACI 440.2R-17 2017) still adopt stress–strain models for FRP-confined concrete that were empirically derived from tests of plain concrete cylinders under concentric axial loading despite the presence of new models that were applied to eccentrically-loaded columns [e.g. (El Maaddawy 2009; Csuka and Kollár 2012; Wu and Jiang 2013; Fahmy and Farghal 2016; Wu and Cao 2017; Cao et al. 2018; Lin and Teng 2019)]. In fact, the illustrious Lam and Teng (2003) stress–strain model

for FRP-confined concrete which was adopted by ACI 440.2R-17 (2017) was derived using a database containing test results of 76 plain concrete circular cylinders confined using different types of unidirectional FRP sheets. The database included cylinders with a height-to-diameter ratio of 2–4, diameters from 100 to 200 mm and unconfined concrete strengths from 26.2 to 55.2 MPa.

Recently, Wu and Jiang (2013) have shown that stress–strain models developed for concentrically-loaded columns cannot be used efficiently to predict column response under eccentric loading and that the stress–strain curve shows a significant stiffening trend with the increase in load eccentricity. Wu and Jiang (2013) concluded that there is no direct relationship between the longitudinal stress and strain in FRP-confined concrete columns under eccentric loading and that both axial load and loading eccentricity affect the stress–strain relationship. To add to the complexity of this controversial issue, Wu and Cao (2017) concluded that the load path used to apply eccentric loading greatly affects the stress–strain behavior of FRP-confined concrete and that different stress–strain models should be used for FRP-confined concrete under different load paths. As a matter of fact, Cao et al. (2018) examined the effect of two different load paths, namely constant axial force with increasing load eccentricity or constant load eccentricity with increasing axial load, on the stress–strain behavior of FRP-confined eccentrically-loaded columns and reported significant differences between the stress–strain relationships in the two cases.

In view of the above-mentioned ambiguities, this research was devised to examine the effect of using two FRP wrapping schemes in terms of fiber orientation (longitudinal versus circumferential) and stiffness of the FRP jacket on the performance of medium-scale RC columns under the combined action of axial compression and bending moments. Tests are also intended to provide experimental evidence for future development of a more realistic stress–strain model for FRP-confined concrete under different P – M interactions. Test results are also used to construct P – M interaction diagrams for the FRP-wrapped columns.

2 Testing Program

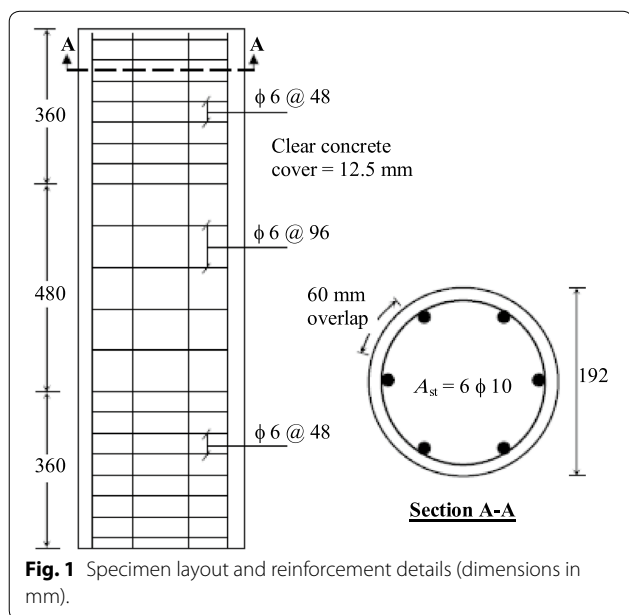
2.1 Specimen Design

To develop a better understanding of the behavior of FRP-wrapped columns under the combined action of axial compression and bending moments, 25 medium-scale circular stocky RC columns with a 1200 mm height and 192 mm diameter were tested. Following ACI 318-14 (2014) provisions, the columns were reinforced with six longitudinal bars of 10-mm diameter at a gross reinforcement ratio of 0.017. Circular steel ties with a bar diameter

of 6 mm were used at 96 mm spacing within the central 480 mm of the column height and at 48 mm within the upper and lower ends of the column as shown in Fig. 1.

Test parameters included the loading combination, absence/presence of an FRP jacket as well as the FRP wrapping system. To examine the effects of loading combination, the 25 test specimens were grouped into 5 categories and were designated with a group number G0, G25, G50, G65 and G_{INF} indicating that columns were tested under axial compression with a loading eccentricity (e) of 0, 25, 50, 65 mm and infinity, respectively. The selected eccentricity values correspond to eccentricity-to-diameter ratios (e/D where D is the diameter of the column cross section) of 0, 0.13, 0.26, 0.34 and infinity, respectively. To assess the effectiveness of different carbon FRP (CFRP) wrapping systems each of the G groups included specimens that were kept unwrapped to serve as control columns and specimens that were fully wrapped using 2 different configurations. In the first configuration designated as C, columns were wrapped with a single ply of the CFRP fabric with the main fibers oriented parallel to the hoop direction, i.e. at 90° to the longitudinal column axis. In the second configuration designated as LC, columns were wrapped with 2 plies of the CFRP fabric with fibers oriented parallel to the column's longitudinal axis in the first ply and parallel to hoop direction in the second thereby providing sufficient anchorage for the longitudinal sheets and preventing premature bonding failure.

Specimen designations used in Table 1 indicate the column group which signifies the loading eccentricity, the absence of an FRP jacket wherein columns were



unwrapped (U), the use of a hoop CFRP ply (C), the use of a longitudinal CFRP ply (L), and a designation A, B or C where duplicate specimens were used. The authors realize that in view of the expected variation in material properties as well as preparation and testing conditions of the different specimens a minimum of three duplicates of each test configuration would be needed to draw definite conclusions on the effect of the various test parameters. However; financial constraints of the current study imposed strict limitations on the number of test specimens and prevented the use of specimen duplicates for specific test configurations.

2.2 Materials

The concrete mix was designed according to ACI 211.1-91 (1991) using ordinary Portland cement (Type I) with a water-to-cement ratio of 0.48. The design mix ratio of cement:fine aggregate:coarse aggregate was 1:1.75:1.47. A mixture of fine limestone aggregate and silica sand, at a proportion of 9:1 by volume, was used as the fine aggregate. Crushed limestone, with a maximum size of 9.5 mm, was used for the coarse aggregate. Flocrete SP33 super plasticizer was used at 1% by cement weight to achieve the required slump. Twelve concrete batches were used to cast the columns. Based on test results of 36 cylinders (150 × 300 mm) that were cast, wet-cured and tested with their companion column specimens, an average compressive concrete strength of about 59 MPa was attained by the time that columns were tested. The concrete compressive strength of the different batches varied between 56.2 and 61.7 MPa with a coefficient of variation (calculated by dividing the standard deviation by the mean and multiplying by 100) of about 3.2.

The longitudinal and transverse column reinforcement were provided using deformed steel bars of 10 mm (with 418 MPa yield strength and 19% elongation) and 6 mm (with 524 MPa yield strength and 15% elongation) diameters, respectively.

High strength unidirectional carbon FRP sheets (MBRACE FIBER CF 230/4900.300g/5.100m) from BASF were used for column jacketing. The 500 mm wide CFRP sheets had a nominal thickness of 0.166 mm, tensile strength of 4900 MPa, 2.1% strain at break and an elastic tensile modulus (E_f) of 230 GPa as provided by the manufacturer. The two-part MBrace Saturant (epoxy resin) was used as the adhesive.

2.3 Specimen Preparation

Test specimens were cast in the upright position using PVC plastic forms. The specimens were cured in their forms for 2 days after which columns were removed from the forms and wet-cured using moist hessian for 26 more days. After completion of the curing process, columns

Table 1 Summary of test results.

Specimen designation ^a	Loading eccentricity (mm)	P_u (kN)	K_i (kN/mm)	Δ_u (mm)	Δ_{max} (mm)	Δ_l (mm)	μ	Toughness (kN mm)	Moment (kN m)
G0-U-A	0	1529	2896	0.76	0.95	–	2.00	715	0
G0-U-B		1573	3692	0.62	0.75		1.82	618	
G0-C-A	0	1930	1986	4.56	4.57	–	5.60	7356	0
G0-C-B		1872 (123) ^b	2027 (61)	2.70 (526)	2.75 (431)		3.67 (243)	3853 (841)	
G0-LC-A	0	1987	2079	4.93	5.36	–	5.91	8335	0
G0-LC-B		2041	2299	3.22	3.93		4.68	5300	
G0-LC-C		2021 (130) ^b	2114 (66)	3.72 (573)	4.07 (524)		3.77 (251)	5517 (957)	
G25-U-A	25	1351	2213	0.82	0.94	2.30	1.80	680	36.9
G25-U-B		1154	2385	0.71	0.76	0.64	1.88	497	29.6
G25-C-A	25	1545	2724	1.27	1.80	7.34	3.50	1397	50.0
G25-C-B		1580 (125) ^b	1912 (101)	1.68 (192)	3.23 (296)	7.32 (499)	3.70 (196)	1862 (277)	51.1 (152)
G25-LC	25	1682 (134) ^b	2070 (90)	1.37 (178)	1.65 (194)	1.89 (129)	2.97 (161)	1542 (262)	45.2 (136)
G50-U-A	50	900	NA	NA	NA	3.34	NA	NA	48.0
G50-U-B		894	1501	0.62	0.65	2.43	1.16	280	46.7
G50-C	50	1210 (135) ^b	2216 (148)	0.83 (134)	1.05 (162)	5.50 (191)	1.94 (167)	639 (228)	67.2 (142)
G50-LC-A	50	1341	1633	1.58	1.61	1.81	1.92	1527	69.5
G50-LC-B		1303 (147) ^b	1603 (108)	1.12 (218)	1.18 (215)	3.80 (97)	1.66 (154)	905 (434)	70.1 (147)
G65-U	65	789	1803	0.63	0.80	3.20	1.92	318	53.8
G65-C	65	1048 (133) ^b	1693 (94)	1.41 (224)	1.59 (199)	8.60 (269)	2.60 (135)	1123 (353)	77.1 (143)
G65-LC	65	1122 (142) ^b	2032 (113)	0.97 (154)	1.20 (150)	7.90 (247)	2.57 (134)	747 (235)	81.8 (152)
G _{INF} -U-A	Infinite	117	20.6	20.47	25.76	–	3.98	2425	22.4
G _{INF} -U-B		125	19.2	17.09	17.82		4.12	1625	24.0
G _{INF} -C-A	Infinite	127	24.4	24.62	24.62	–	6.84	2505	24.4
G _{INF} -C-B		134 (108) ^b	22.4 (118)	28.24 (141)	28.24 (243)		5.98 (158)	3158 (140)	25.7 (108)
G _{INF} -LC	Infinite	260 (215) ^b	24 (121)	16.14 (86)	16.14 (74)	–	2.17 (54)	2492 (123)	49.9 (215)

NA: Axial displacement measurements were dismissed for this specimen.

^a G0, G25, G50 and G65 is the group designation indicating the loading eccentricity in mm; G_{INF} is the group designation indicating column tested in pure bending; U: Unwrapped specimen; C: Column wrapped with a circumferential CFRP ply; LC: Column wrapped with two CFRP plies: one longitudinal and another circumferential.

^b Numbers between brackets in this row are computed as the ratio of the response parameter (average value in case of specimen duplicates) to that of the control unwrapped companion specimen (average value in case of specimen duplicates) tested under the same load eccentricity, expressed as a percent.

were kept in the open lab environment in preparation for jacketing. A total of 16 specimens were strengthened using one of the 2 wrapping systems described earlier, namely the C and LC configurations. On average, the FRP jacketing started 1 week after the 28-day curing stage.

To ensure successful bonding of the FRP fabric to concrete surfaces, column surface irregularities were corrected and large pores (if any) were filled with a dental plaster material (pro dental stone). Following BASF instructions, concrete surfaces were cleaned and prepared to receive the adhesive. The two adhesive parts (resin and hardener) were mechanically mixed, at a ratio of 2:1 by weight, and then spread uniformly over the surface at a quantity of 1.2 kg/m² (0.7 kg/m² was used for multiple layers). The pre-cut CFRP sheets were applied to the saturant-coated concrete surface

using a hand lay-up method. FRP sheets were attached to the concrete surface and squeezed in a direction parallel to fiber orientation using a defoaming roller to ensure full impregnation of the fabric with the resin and to remove any entrapped air. Where a second FRP layer was required, the MBrace Saturant was brushed onto the cut fabric which was then laid onto the first layer of FRP sheets.

A 100-mm overlap length along the hoop direction and a 20-mm overlap length in the axial direction were maintained for the hoop FRP wraps. Overlap length for the longitudinal FRP sheets along the hoop direction was kept at 20 mm. In view of the expected stress concentrations at column ends, all columns including the control specimens were confined with additional 200 mm-wide hoop FRP sheets at both ends.

2.4 Test Procedures and Instrumentation

Column specimens (G0 to G65) were tested under axial compression with variable eccentricities using a 4000 kN Universal Testing Machine. Compression tests started 1 month, on average, after the columns have been jacketed. The axial load was applied using displacement control, at a rate of 0.5 mm/min, to monitor column response beyond peak capacity. The monotonic axial loading was gradually increased until failure. A set of steel loading plates was fabricated for the application of axial compression at the desired eccentricity: a top plate with a knife-edge that was fastened to the loading jack and a bottom adapter plate that was placed directly on top of the specimen. The top plate was designed to transfer the compressive load from the hydraulic jack to the adapter plate. Several V-notch grooves were cut on the top surface of the 40-mm thick adapter plate to transfer the load from the knife-edge to the test specimen at the required eccentricity as shown in Fig. 2a. Rigid steel collars, 200 mm-wide, were used to confine the upper and lower ends of the G50 and G65 columns to prevent premature failure at these locations which would be otherwise expected in view of stress concentration near points of application of loading. A gap of about 20 mm was maintained between the steel collars and the end surfaces of the test specimen to avoid direct loading of the collars and prevent any interference with the end conditions (pinned at the top-fixed at the bottom). The authors have not observed any other effect of the collars on column response.

Using the compressometer-extensometer measurement system shown in Fig. 2a, each of the G0 to G65 columns was instrumented with 3 linear variable differential transformers (LVDTs). The L1 and L2 transducers, with a gage length of 450 mm, were centered at column mid-height to measure axial displacements at the compression and tension column sides. The L3 transducer was mounted onto the extensometer to measure hoop strains at mid-height.

In view of the loading conditions of G0, G25, G50 and G65 columns, the maximum lateral deflections were expected to take place within the upper half of the column rather than at column mid-height. Because of budget constraints and limitations of the testing facility, multiple measurements of lateral deflections over the height of the test columns were not possible. As a result, lateral deflections were measured using a single LVDT (L4) that was mounted at a fixed position in all specimens regardless of changes in the locus of maximum displacement as a result of the change in eccentricity of the applied loading. Lateral deflections were recorded using the L4 transformer at about 500 mm measured from the column's upper end. However, it is important to note that when columns are designed as stocky (non-slender)

columns as in this study the development of secondary moments induced by lateral buckling, and hence the variation of total moments over the height of the column would be limited. As such, the maximum moments experienced by the test specimens are not expected to significantly deviate from the total ultimate moments (primary plus secondary) computed in Sect. 3.5 at the location of the L4 transformer.

On the other hand, G_{INF} specimens were tested in pure bending using the 4-point bending test shown in Fig. 2b with a shear span of about 384 mm measured from the hinge support to the loading point. The LVDT (L5) shown in Fig. 2b was used to measure mid-span deflections. Load and displacement measurements were recorded using data acquisition software at a rate of five readings per second.

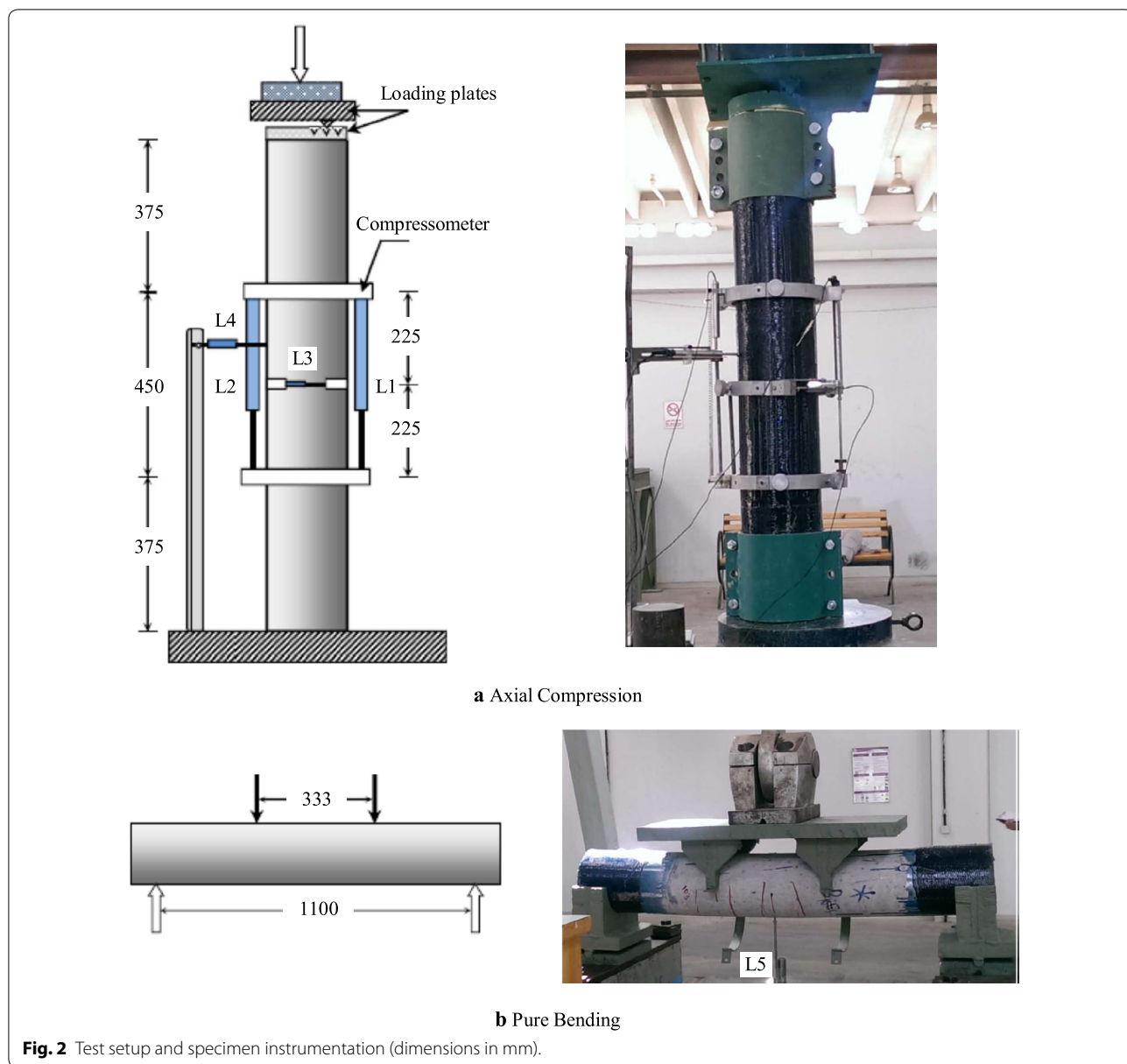
3 Experimental Results and Discussion

3.1 General

In view of test results and the argument of stability and consistency of displacement and strain readings at the loading position described by Wu and Jiang (2013), the axial displacement value (Δ) reported hereinafter is the displacement at the loading position as calculated from L1 and L2 readings using linear interpolation.

To assess column behavior a number of response parameters, whose values are presented in Table 1, were defined based on the experimental axial force–displacement (P – Δ) relationships shown in Fig. 3. The tabulated values for P_u denote the ultimate resistance or axial load-carrying capacity; Δ_u is the corresponding axial displacement whereas the displacement value Δ_{max} corresponds to the strength failure state as observed experimentally. The initial secant stiffness (K_i) defines the slope of a straight line connecting the origin with a point on the P – Δ curve whose ordinate equals $0.5P_u$.

Each of the experimental P – Δ curves was replaced with a bilinear curve in order to define the yield point (P_y, Δ_y) as shown in Fig. 4. The yield force P_y was determined using an iterative procedure to arrive at a value that does not exceed P_u and that satisfies an equal area criterion wherein the area under the bilinear P – Δ curve approximates that under the actual curve up to the point of strength failure. The P_y value is accepted only if a point with an x-coordinate smaller than Δ_y but with a y-coordinate that equals $0.6P_y$ can be found on the actual P – Δ curve. The first segment of the bilinear curve connects origin to the assumed yield point passing through the point with an ordinate of $0.6P_y$ whereas the second segment extends from the assumed yield point to the point of strength failure. Subsequently, the global displacement ductility (μ) for a specific column is calculated as the maximum-to-yield displacement



ratio (Δ_{max}/Δ_y). Toughness values, on the other hand, denote the area under the experimental $P-\Delta$ curve up to the point of strength failure thereby characterizing column's capacity to dissipate energy. The lateral displacements (Δ_l) reported in Table 1 represent the ultimate L4 transducer readings.

Unfortunately, a malfunction of the L3 displacement transducer was only noted during the stage of data analysis. As such, hoop deformations were discarded.

The same set of parameters was used for the G_{INF} specimens tested in pure bending (see Fig. 2b) but in this case

P_u was used to define the ultimate load which is applied perpendicular, rather than parallel, to the longitudinal axis of the specimen whereas Δ was used to designate mid-span deflections as measured by the L5 transducer shown in Fig. 2b.

3.2 Failure Modes

Figure 5 displays damage patterns in a number of test specimens. Except for the G_{INF} specimens, columns were vertically aligned in the testing machine simulating casting position. A typical crushing failure at column

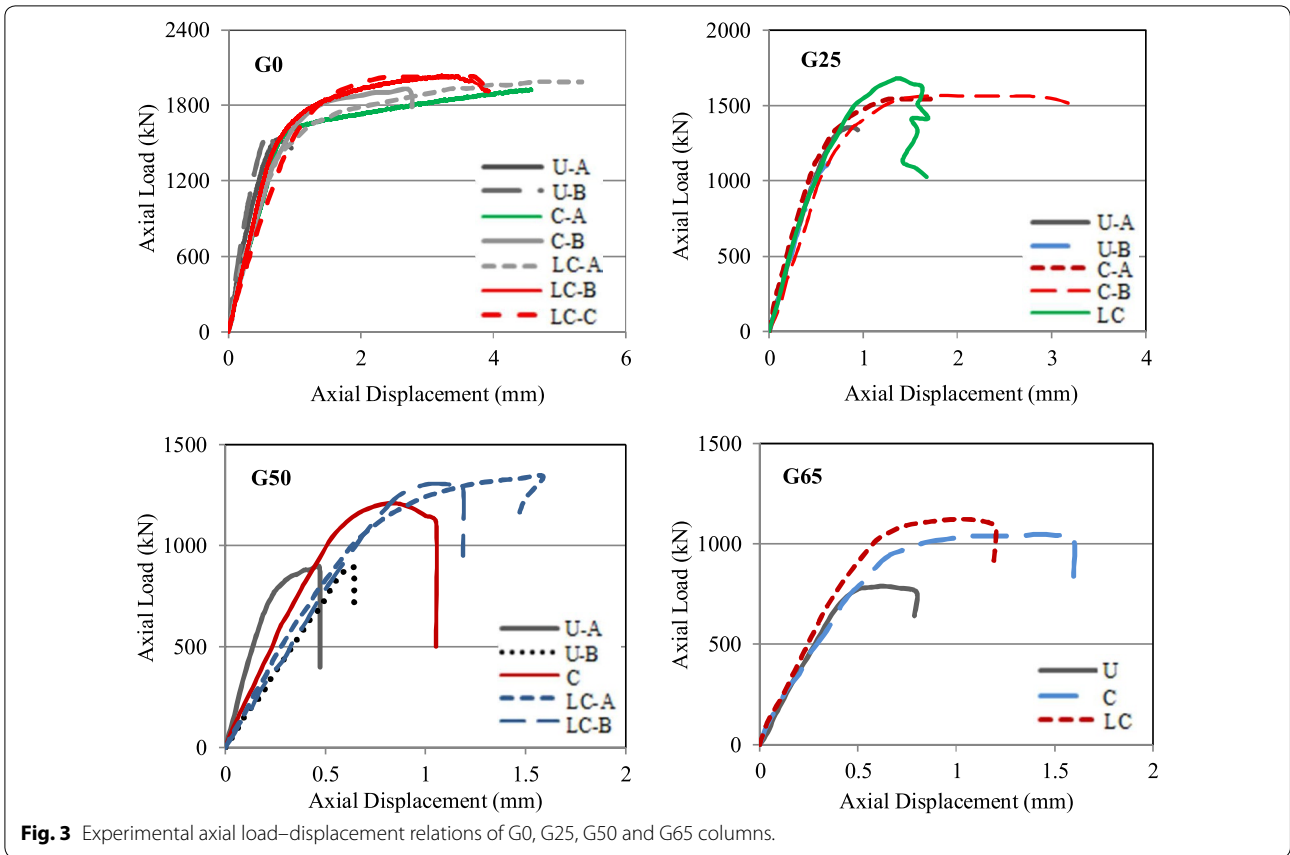


Fig. 3 Experimental axial load–displacement relations of G0, G25, G50 and G65 columns.

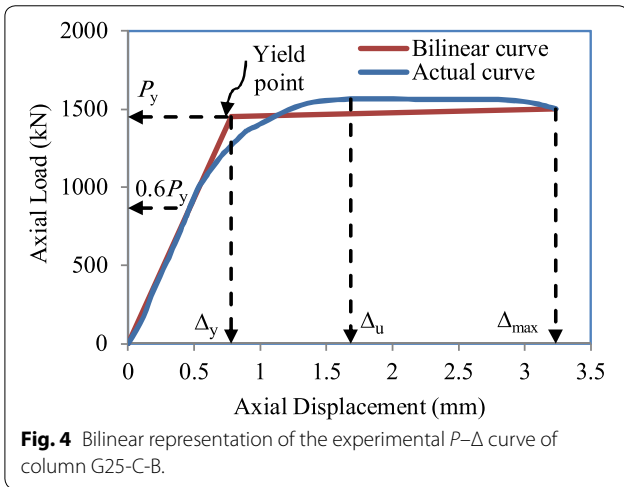


Fig. 4 Bilinear representation of the experimental $P-\Delta$ curve of column G25-C-B.

mid-height occurred in all concentrically- and 25 mm eccentrically-loaded columns. As the level of loading eccentricity increased, location of failure (as noted under the $0.26D$ and $0.34D$ eccentric loading) migrated towards the upper steel collar as a result of stress concentrations in this region. Column failure was associated with

crushing of concrete in the compression side accompanied by local buckling of the longitudinal reinforcement bars. Tensile cracks were observed at the tension surface of eccentrically-loaded columns. Column buckling was observed in all eccentrically-loaded columns and was more noticeable at higher load eccentricities. In FRP-wrapped columns, crushing of concrete resulted in rupture (perpendicular to hoop direction) of the FRP sheets whereas the tensile concrete cracking was reflected through circumferential cracks in the FRP sheets themselves. Despite the enhancement in member ductility observed in FRP-wrapped columns compared to their companion unwrapped columns, failure itself was more sudden and explosive.

Flexural cracks were noticed within the middle region of G_{INF} specimens tested in pure flexure. Cracks originated at the bottom surface of the specimen and increased in number and width while propagating towards the upper surface as the level of bending moment increased. This was followed by sudden concrete crushing (secondary compression failure) in the upper region/surface of the unwrapped specimens. CFRP confinement limited the extent of observed flexural cracking.



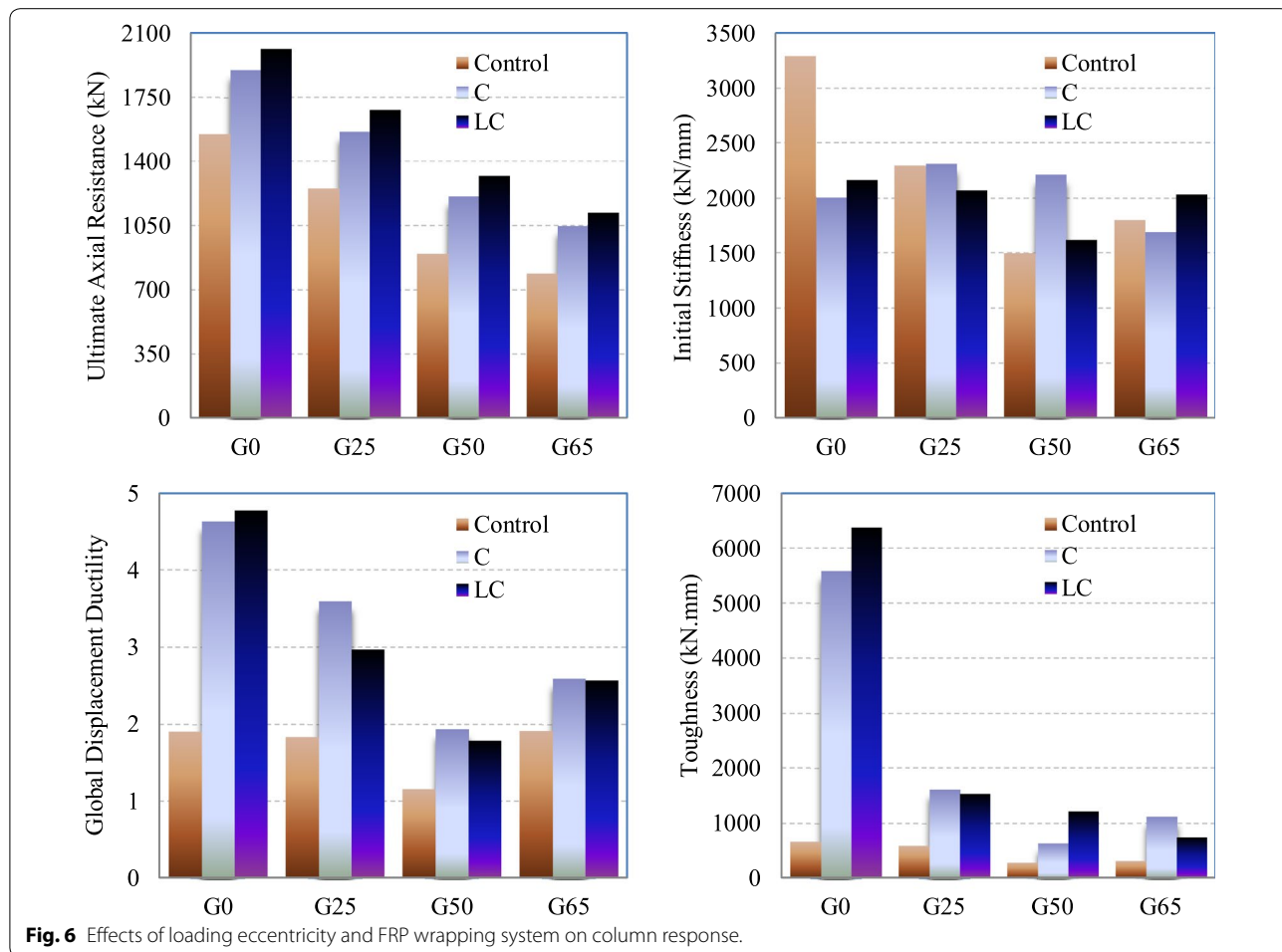
Fig. 5 Examples of observed failure patterns in test specimens.

Post inspection of the FRP jackets confirmed proper lamination of the FRP sheets. Examination of the FRP sheets at locations of rupture revealed that a thin layer of concrete was attached to the inner surface of the sheets thereby indicating proper bonding and thus full activation of the fabric sheets. Adequacy of the adopted overlapping system was confirmed during the tests. Delamination of the FRP sheets was not observed at the overlapping zones.

3.3 Effects of Loading Eccentricity

Columns in real life are typically subjected to the combined action of axial compression and bending moments. Keeping in mind the limited number of test specimens and the lack of specimen duplicates for specific test configurations, general effects of the increase in bending moments (i.e. in loading eccentricity) on the response of test columns are deployed in Fig. 6. In conjunction with the values presented in Table 1, Fig. 6 deploys a sizeable yet negative effect of the increase in loading eccentricity on axial resistance of the control

unwrapped columns as well as the C and LC wrapped columns. However, observed reductions in axial resistance with the increase in load eccentricity were found to be less pronounced for FRP-wrapped columns than for unwrapped columns. While a loading eccentricity of $0.26D$ reduced the ultimate resistance of control columns by 42%, the use of FRP jackets resulted in slightly higher resistance limiting strength reductions to about 35% only. Even at a loading eccentricity of $0.34D$, strength reductions of about 49% were recorded for unwrapped columns in comparison to 45% for FRP-wrapped columns. One should note that Bisby and Ranger (2010) made exactly the opposite observation leading them to suggest that member reduction factors used in current design practices to account for the effect of accidental load eccentricities need to be decreased for FRP-confined columns. Of course, this controversy in test results reported by different researchers can be explained in view of, among other factors, the differences in geometrical and material properties of the test specimens as well as in loading conditions.



The increase in loading eccentricity had similar negative effects on initial stiffness of the control columns resulting in a decrease of about 45% at an eccentricity of $0.34D$ however; column jacketing with FRP sheets almost diminished this negative effect on column stiffness. Nonetheless, the effects of FRP-jacketing on the initial stiffness of test specimens under a specific loading eccentricity were inconclusive as can be seen in Table 1 and Fig. 3. The reader should note that researchers [e.g. (Wu and Jiang 2013)] have recognized that FRP jacketing has no tangible effect on the initial elastic modulus of FRP-confined concrete as FRP confinement would not be activated in the initial stages of loading, i.e. no confinement pressure would be exerted on the concrete. Inescapable variations between the different specimens in a specific test configuration may have also contributed to the notable variance in stiffness values. However, the anomaly observed in the case of the G50 specimens where one of the control unwrapped specimens (G50-U-A) shows a much larger stiffness compared to the companion specimens tested under the same loading eccentricity suggests that a malfunction of the L1 and/or L2 transducers may have taken place during the test. As such, response parameters associated with the L1 and L2 readings have been dismissed for this specimen as noted in Table 1. On the other hand, increases in bending moments also reduced axial ductility (up to 39%) and toughness (up to 58%) of the control columns with much higher reductions noted in the FRP-jacketed columns as associated with the ability of FRP sheets to enhance the axial and flexural column rigidities.

3.4 Effects of Wrapping System

Results presented in Table 1 confirm the efficiency of FRP hoop confinement (the C configuration) in increasing the axial load-carrying capacity of test columns. Increases of about 20% were recorded for the concentrically-loaded columns and for those loaded at an eccentricity of $0.13D$. Larger enhancements reaching up to 44% (33%) were noted in the G50 (G65) columns loaded at an eccentricity of $0.26D$ ($0.34D$). The passive confinement provided by the hoop FRP sheets allowed the eccentrically-loaded G25, G50 and G65 columns to attain higher axial resistance as they deformed laterally with increases of lateral deformation ability reaching up to 5, 2 and 3 times that of their companion unconfined columns, respectively. Similar increases in lateral deformation ability of hoop FRP-confined columns were reported by Al-Nimry and Soman (2018). Whilst the C configuration resulted in significant enhancements in axial deformation ability, ductility and toughness of the concentrically loaded columns, the beneficial confinement effects tended to decrease with the increase in bending moments.

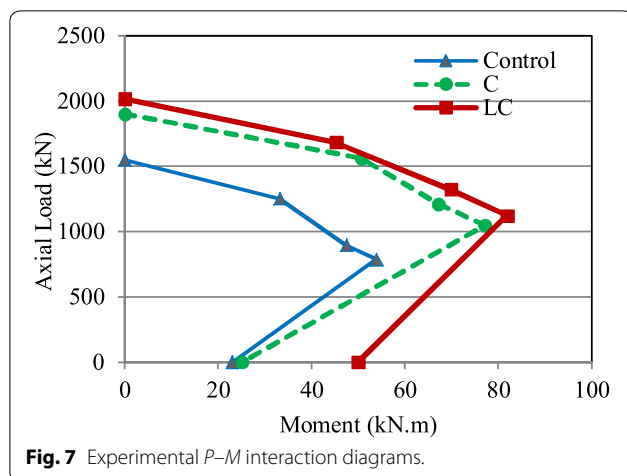
Compared to control unwrapped columns, the use of longitudinal FRP reinforcement as per the LC configuration resulted in substantial improvements in axial strength amounting to a total of 30, 34, 47 and 42% in the G0, G25, G50 and G65 columns, respectively. This wrapping system allowed columns to resist higher axial loads while increasing their flexural rigidity i.e. limiting their lateral deformability compared to companion columns wrapped with hoop FRP sheets only. The LC wrapped columns sustained higher axial displacements at ultimate resistance and recorded higher ductility and toughness compared to their companion controls. Similar to the hoop FRP confinement system, efficiency of the LC wrapping system tended to decrease with increasing levels of the loading eccentricity as can be clearly seen in Fig. 6. On the other hand, toughness of the C and LC wrapped columns tested in pure compression reached 8.4 and 9.6 times, respectively that of the companion control columns whilst ductility reached about 2.5 times that of the control columns. Although the enhancements in ductility (and toughness) of the FRP-jacketed columns decreased with the increase in applied bending moments, substantial enhancements were noted at loading eccentricities of $0.34D$ amounting to 34% (and 135%) in specimens wrapped with the LC configuration.

The P_u values reported in Table 1 show that the LC wrapping system introduced slight enhancements, past those achieved via the C confinement system, in axial column strength reaching 7.6, 9.3 and 7.1% for the G25, G50 and G65 columns, respectively whilst limiting ultimate lateral deformations that were reduced by 74, 49 and 8%, respectively.

In pure flexure, hoop FRP confinement provided by the C wrapping system resulted in a minor increase of about 8% in flexural resistance accompanied with an increase in lateral deformation ability of about 41% compared to the unwrapped control specimen leading to an increase of about 58% in ductility. Compared to their companion unwrapped specimens, using the LC wrapping system significantly enhanced (more than doubled) the specimen's flexural capacity while reducing ultimate mid-span deflections by 14% thereby signifying tangible improvements in flexural rigidity. This increase in flexural stiffness of the FRP wrapped specimen had a drastic effect on ductility resulting in reductions of about 46% compared to that attained by the companion control specimens.

3.5 Experimental $P-M$ Interaction Diagrams

Based on test results, $P-M$ interaction diagrams were constructed for the control unwrapped and FRP wrapped columns as shown in Fig. 7. Each $P-M$ curve consists of a series of straight lines connecting 5 points whose coordinates represent average $P-M$ capacities of the relevant



specimens tested under compression loading at 0, $0.13D$, $0.26D$, $0.34D$ loading eccentricities and in pure bending, i.e. at infinite eccentricity.

The first point, from left to right, on the P – M interaction diagram corresponds to the column tested under axial compression at zero eccentricity (i.e. pure compression, $M=0$) wherein the whole concrete section is considered to be under compression and the axial force is the load-carrying capacity (P_u) of the G0 columns reported in Table 1.

The 2nd, 3rd and 4th points on the curve have ordinate values equal to the axial load-carrying capacity of the column, i.e. P_u value of the G25, G50 and G65 columns, respectively whilst the abscissa M_i is the accompanying ultimate moment capacity. The ultimate moment capacities reported in Table 1 are the product of the P_u value and the total eccentricity ($e + \Delta_l$) where e is the loading eccentricity and Δ_l is the lateral deflection of the column at ultimate resistance as measured by transducer L4 (see Fig. 2a) at about 500 mm from the upper column end thereby incorporating secondary moments. Once again, as the L4 measurements do not necessarily represent maximum values of lateral deflection, ordinates of the 2nd, 3rd and 4th points of the experimental P – M curves are expected to be slightly smaller than the actual moment resistance of the test columns. The 5th point on the curve corresponds to the G_{INF} columns tested in pure bending under zero axial force. The moment capacity in this case is the product of support reaction, which is half the applied ultimate load in the 4-point flexural test shown in Fig. 2b, and the distance from support to point load.

The three experimental P – M interaction diagrams shown in Fig. 7 clearly display the beneficial effects of the two FRP wrapping systems considered in this study. In fact, Fig. 7 shows that the C and LC wrapping

arrangements have a significant, almost similar, positive impact on the column capacity to resist bending moments up to the maximum loading eccentricity considered in this study (pure bending being excluded) of about $0.34D$. One should note that strength improvements beyond this point, if any, were not investigated. Nonetheless, this observation means that strength enhancement could be realized even in cases where compression is no longer the dominant failure mode contrary to what is implicated in international design guidelines [e.g. (ACI 440.2R-17 2017)]. Compared to unconfined specimens, slight enhancements in flexural strength of about 8% were noted in hoop FRP-confined columns tested in pure bending. Conversely, using longitudinal FRP sheets confined with hoop wraps provided considerable flexural resistance in columns subjected to pure bending; compared to unwrapped specimens, this wrapping system managed to double the flexural resistance of columns.

4 Theoretical P – M Interaction Diagrams

4.1 Background

Few researchers have produced theoretical axial force-bending moment interaction diagrams [e.g. (Bisby and Ranger 2010; Fitzwilliam and Bisby 2010; Chaallal and Shahawy 2000; Nanni and Norris 1995; Di Nardo et al. 2006)] for FRP-jacketed columns. In 2009, Rocca et al. (2009) proposed a method to construct simplified P – M interaction diagrams that could be used for practical design applications of FRP-wrapped RC columns of circular and non-circular cross-sections.

In this section, theoretical P – M interaction curves are constructed for FRP-wrapped columns using the C and LC wrapping systems. Each of the P – M curves includes 3 distinct points representing the P – M coordinates for the column under: (a) pure compression loading; (b) balanced condition; and (c) pure flexural loading as for a beam in simple bending with zero axial force.

4.1.1 Point 1: Pure Compression

In this case the bending moment is zero. The whole section is under compression and the uniform strain in the concrete is set to $\varepsilon_{cu} = 0.003$ for the unconfined section and ε_{ccu} (as defined later) for the FRP-confined section. The compressive strain in the six longitudinal steel bars ε_s is assumed to have reached the yield strain ε_{sy} ($= 0.002$).

4.1.2 Point 2: Balanced Failure

Strains vary linearly across the section with the depth to the neutral axis (c) equal to the balanced value c_b . The value of c_b is calculated using similar triangles with the concrete strain in the outermost fiber on the compression face equal to the maximum usable strain of 0.003,

or ϵ_{ccu} if FRP confinement is used, and the strain in the outer most steel nearest to the tensile face equal to the yield strain value of 0.002.

4.1.3 Point 3: Pure Bending

The axial force is zero. Strains vary linearly with the maximum concrete strain equal to ϵ_{cu} or ϵ_{ccu} as applicable and the strain in the outer most steel in tension is greater than 0.002.

4.1.4 Point *i*: Any Other Point

The $P-M$ coordinates for any other point on the interaction curve depend on its location with respect to the balanced condition or state. If the depth to the neutral axis is larger than c_b then the section is compression-controlled with strain in the outer most tension steel (ϵ_s) less than ϵ_{sy} . On the other hand, if the c value is less than c_b then the strain in the outer most tension steel exceeds ϵ_{sy} . The section would be tension-controlled only when a tensile strain of 0.005 is reached in the reinforcing bars nearest to the tensile face. In any case, the strain in the farthest concrete fiber in the compression part of the section is assumed to have reached ϵ_{cu} or ϵ_{ccu} as applicable.

4.1.5 $P-M$ Values

The $P-M$ values corresponding to a specific point on the interaction diagram are calculated using conventional section analysis and assuming linear variation in concrete strains across the column section as shown by the strain profile in Fig. 8. To this end, concrete in the compression zone (lightly shaded area in the cross section of Fig. 8) is divided into 8 segments of equal width. The concrete strain value ϵ_{ci} at the center of the i th segment ($i=1$ to 8) is then determined using linear trigonometry and the corresponding concrete stress f_{ci} is calculated using the relevant stress-strain model of FRP-confined concrete as described in Sects. 4.2 and 4.3. As usual, contribution of concrete in tension is conservatively neglected. Assuming perfect bond, strains in the steel bars are considered equal to those in the adjacent concrete. The steel stress f_{si} is assumed positive for bars in compression and is computed using the actual stress-strain relation of the main reinforcing steel bars as obtained from laboratory tests thereby including the effects of strain hardening.

Force equilibrium requires that,

$$P_{theo} = \sum_{i=1}^8 A_{ci}f_{ci} + A_{s1}f_{s1} + A_{s2}f_{s2} \pm A_{s3}f_{s3} \pm A_{s4}f_{s4} \tag{1}$$

where A_{ci} is the area of the i th concrete segment, f_{ci} is the calculated concrete stress at the centroid of the i th segment, A_{s1} to A_{s4} are areas of the steel reinforcing bars (A_{s1}

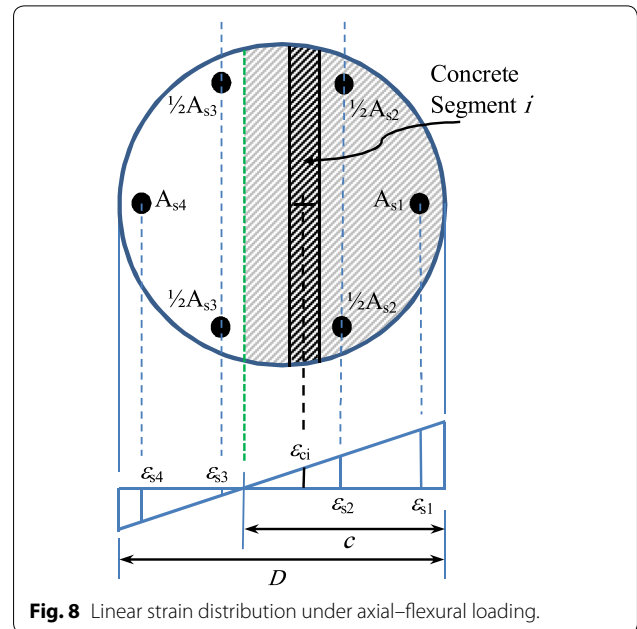


Fig. 8 Linear strain distribution under axial-flexural loading.

and A_{s4} correspond to a single bar whereas A_{s2} and A_{s3} correspond to 2 bars) and f_{s1} to f_{s4} are the corresponding steel stress values.

On the other hand, moment equilibrium gives,

$$M_{theo} = \sum_{i=1}^8 A_{ci}f_{ci}S_{ci} + A_{s1}f_{s1}S_1 + A_{s2}f_{s2}S_2 \pm A_{s3}f_{s3}S_3 \pm A_{s4}f_{s4}S_4 \tag{2}$$

where S_{ci} is the distance from column centroid to the centroid of segment i and S_1 , S_2 , S_3 and S_4 are the distances from column centroid to the steel bars 1, 2, 3 and 4, respectively.

Effects of longitudinal CFRP sheets, used in the LC wrapping system, on column response are introduced into the equilibrium equations as follows

$$P_{theo} = \sum_{i=1}^8 A_{ci}f_{ci} + A_{s1}f_{s1} + A_{s2}f_{s2} \pm A_{s3}f_{s3} \pm A_{s4}f_{s4} - A_v f_{FRP} \tag{3}$$

$$M_{theo} = \sum_{i=1}^8 A_{ci}f_{ci}S_{ci} + A_{s1}f_{s1}S_1 + A_{s2}f_{s2}S_2 \pm A_{s3}f_{s3}S_3 \pm A_{s4}f_{s4}S_4 + A_v f_{FRP} z \tag{4}$$

where A_v is the area of FRP sheets on tension face of the eccentrically-loaded column and is calculated using the geometric properties of a circular segment (depending on the position of the neutral axis) with a thickness equal to the nominal thickness of the FRP sheets, f_{FRP} is the tensile strength of FRP sheets (4900 MPa as provided by

the manufacturer) and z is the distance measured from column centroid to the centroid of FRP sheets (center of arc in this case).

4.2 Stress–Strain Model

The stress–strain model developed by Lam and Teng (2003) is used herein to assess the confinement-induced improvement in the strength of FRP-confined compression sections as proposed by ACI 440.2R-17 (2017). The model, shown in Fig. 9a, is given by the following expressions:

$$f_c = \begin{cases} E_c \varepsilon_c - \frac{(E_c - E_2)^2}{4f'_c} \varepsilon_c^2 & 0 \leq \varepsilon_c \leq \varepsilon'_t \\ f'_c + E_2 \varepsilon_c & \varepsilon'_t \leq \varepsilon_c \leq \varepsilon_{ccu} \end{cases} \quad (5a)$$

$$E_2 = \frac{f'_{cc} - f'_c}{\varepsilon_{ccu}} \quad (5b)$$

$$\varepsilon'_t = \frac{2f'_c}{E_c - E_2} \quad (5c)$$

in which f_c and ε_c are the axial stress and axial strain of concrete, respectively, E_c is the elastic modulus of unconfined concrete, E_2 is the slope of the second linear portion of the stress–strain curve, ε'_t is the transition strain, ε_{ccu} is the ultimate axial strain of confined concrete, f'_c is the unconfined cylinder compressive strength of concrete and f'_{cc} is the maximum FRP-confined concrete compressive strength as given by Eq. 6 for circular cross-sections.

$$f'_{cc} = f'_c + \psi_f 3.3f_l \quad (6)$$

where the reduction factor ψ_f is taken as 0.95 and the maximum confinement pressure f_l is given by Eq. 7.

$$f_l = \frac{2E_f n t_f \varepsilon_{fe}}{D} \quad (7)$$

In Eq. 7, E_f is the tensile elastic modulus of FRP sheets, n is the number of FRP plies, t_f is the nominal thickness of one FRP ply, D is the diameter of the column cross section and ε_{fe} is the effective strain in the FRP at failure and is given by Eq. 8.

$$\varepsilon_{fe} = \kappa_\varepsilon \varepsilon_{fu} \quad (8)$$

According to ACI 440.2R-17 (2017), the strain efficiency factor κ_ε is conservatively set at 0.55 to account for premature failure of the FRP jacket, and ε_{fu} is the ultimate strain of FRP sheets. The latter value is determined by multiplying the ultimate strain value provided by the manufacturer by an environmental reduction factor which is set to 0.95 for interior exposure conditions. Moreover, ACI 440.2R-17 (2017) suggests using a minimum confinement ratio f_l/f'_c of 0.08 to ensure a non-descending second branch of the proposed stress–strain curve. The maximum compressive strain in the FRP-confined concrete ε_{ccu} is given as follows:

$$\varepsilon_{ccu} = \varepsilon'_c \left(1.5 + 12\kappa_b \frac{f_l}{f'_c} \left(\frac{\varepsilon_{fe}}{\varepsilon'_c} \right)^{0.45} \right) \leq 0.01 \quad (9)$$

where the maximum strain of unconfined concrete ε'_c is taken as $0.000937(f'_c)^{0.25}$ (Popovics 1973) and the efficiency factor for FRP reinforcement κ_b is taken as 1 for circular cross-sections.

When the eccentricity present in the member does not exceed $0.1D$, Eq. 10 can be used to estimate the nominal axial compressive strength P_o of a normal weight concrete column confined by hoop FRP sheets (ACI 440.2R-17 2017).

$$P_o = 0.85f'_{cc}(A_g - A_{st}) + f_y A_{st} \quad (10)$$

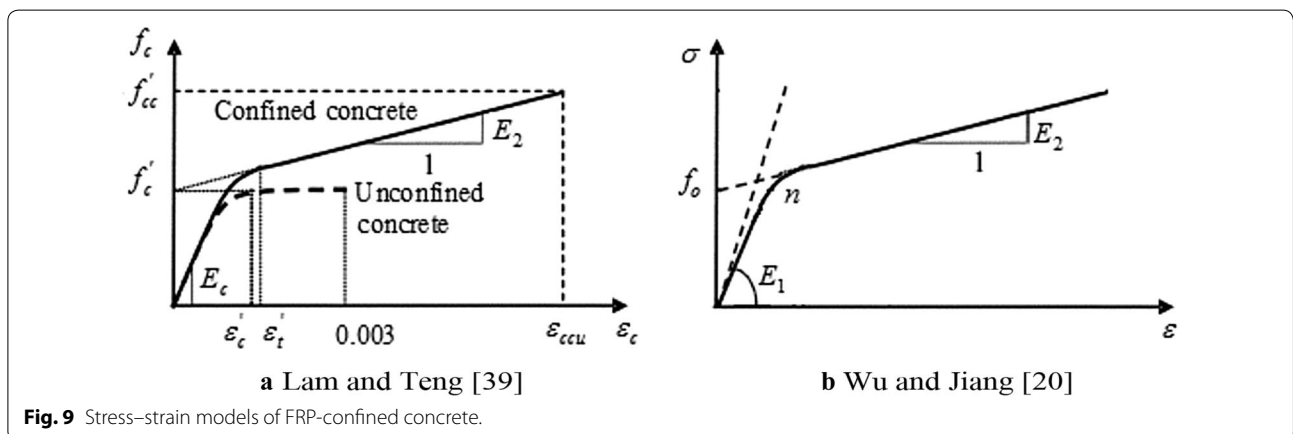


Fig. 9 Stress–strain models of FRP-confined concrete.

where A_g is the gross concrete area and A_{st} is the area of longitudinal reinforcement.

On the other hand, when the loading eccentricity exceeds $0.1D$ as is the case for the 25, 50 and 65 mm eccentricities considered in this study, the ACI 440.2R-17 (2017) permits using the stress–strain relation described by Eq. 5 to define the material properties of the concrete part under compression. In members subjected to axial compression and bending moments, ACI 440.2R-17 (2017) ensures the shear integrity of the confined concrete by limiting the effective strain in the FRP at failure to a maximum value of 0.004 and suggests that strength enhancement should only be considered in members where compression failure is the controlling mode.

4.3 Theoretical vs. Experimental P–M Diagrams

Using the ACI 440.2R-17 (2017) guidelines to predict column capacities under pure compression was found to be reasonable as it slightly overestimates (by about 5%) the P_o value computed using Eqs. 6 and 10 for the FRP-confined columns and exactly predicts that of the FRP-jacketed columns with the LC wrapping system.

Four theoretical P – M curves were developed for the FRP-jacketed columns using the Lam and Teng (2003) stress–strain model with the following considerations:

1. The effective strain in the hoop FRP sheets was limited to a maximum value of 0.004 as per the guidance of ACI 440.2R-17 (2017).
2. The 0.004 limitation was disregarded. In this case ϵ_{fu} was set equal to the value given by the manufacturer and the 0.95 environmental reduction factor was ignored resulting in an effective strain of about 0.012 in the FRP sheets.
3. In view of the fact that premature failure of the FRP system was not experienced in the experimental program; the effective strain in the FRP at failure was assumed to have reached the 0.021 rupture strain given by the manufacturer, i.e. $\kappa_\epsilon = 1$.
4. In addition to the 0.021 rupture strain used in item 3, an ultimate axial strain ratio (UASR) between eccentric loading and concentric loading of 1.5 was assumed. This increase in ultimate axial strain under eccentric loading is based on the observation made by Wu and Jiang (2013) wherein an ultimate strain ratio of 1.56 was reported between an eccentric loaded column and the corresponding concentric loaded column regardless of the eccentricity-to-diameter ratio.

Figure 10 displays the four P – M interaction curves predicted using conventional section analysis in conjunction

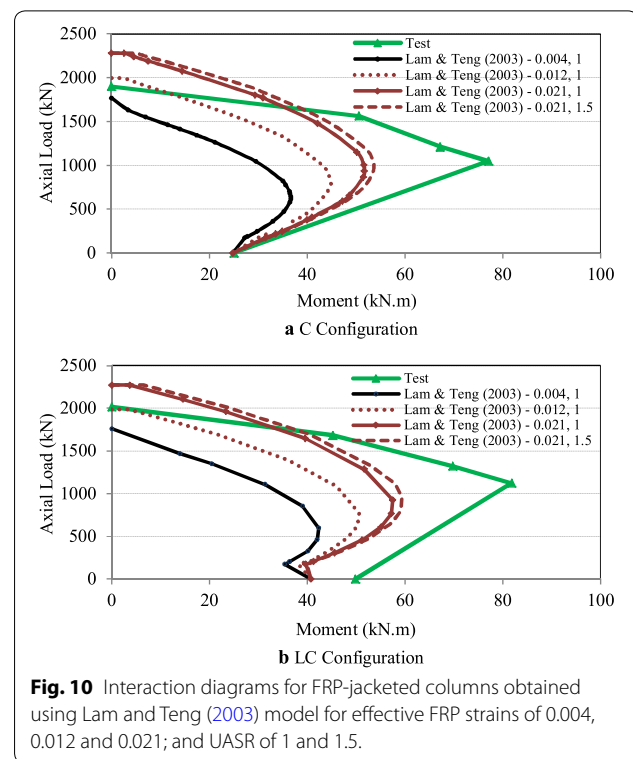


Fig. 10 Interaction diagrams for FRP-jacketed columns obtained using Lam and Teng (2003) model for effective FRP strains of 0.004, 0.012 and 0.021; and UASR of 1 and 1.5.

with the Lam and Teng (2003) stress–strain model under the constraints described earlier. Whilst column strength in pure compression was computed using Eq. 10, the columns were considered to be unconfined under lower axial force levels ($P \leq 0.1 f'_c A_g$) and the flexural strength in pure bending was computed accordingly. Inspection of Fig. 10 reveals that implementing the 0.004 upper bound on the effective strain level in the FRP at failure results in an underestimation of the actual moment resistance under a specific axial force for the 4 axial–flexural load combinations used in the experimental program (pure compression being excluded). Even when discarding the ACI 440.2R-17 (2017) limitation on the effective strain of the FRP jacket, i.e. overriding the maximum limit of 0.004 and thereby increasing the confinement ratio to about 0.08, the theoretical moment strength values are still found to be conservative. This observed discrepancy in moment capacities agrees with the findings of Bisby and Ranger (2010) while opposing the findings of Chaallal and Shahawy (2000) as well as Pham et al. (2013) for FRP-confined columns subjected to large load eccentricities. Again, it should be pointed out that the FRP-jacketed columns in this study were considered to be sufficiently confined by the hoop FRP sheets although the actual confinement ratio computed using an effective strain of 0.004 did not meet the minimum design requirement of 0.08 mentioned earlier. If strength enhancements were to be disregarded as

recommended by ACI 440.2R-17 (2017), lower theoretical $P-M$ values would have been expected thereby increasing the observed differences between theoretical and experimental moment resistance at the same level of axial force. Nonetheless, comparison of the 4 theoretical $P-M$ curves shown in Fig. 10 with their experimental counterpart reveals that using a strain efficiency factor of unity and an ultimate axial strain value of 1.5 times that estimated using Eq. 9 could lead to better predictions of the flexural strength of FRP-jacketed columns under e/D ratios exceeding 0.1 but would tend to overestimate the axial resistance under small load eccentricities ($e/D < 0.1$).

To further examine the appropriateness of using the stress-strain model adopted by ACI 440.2R-17 (2017) in predicting strength enhancements in FRP-confined columns under eccentric loading, $P-M$ interactions for the FRP-jacketed columns were re-evaluated using two recent models that were proposed for eccentrically-loaded columns: namely the eccentricity-dependent model proposed by Wu and Jiang (2013) in 2013 and that proposed by Lin and Teng (2019) in 2019.

The eccentricity-dependent Wu and Jiang (2013) model adopts the stress-strain function given by Eq. 11.

$$\sigma_z = \left[(E_1 \varepsilon_n - f_o) e^{-\varepsilon_z / \varepsilon_n} + f_o + E_2 \varepsilon_z \right] \left(1 - e^{-\varepsilon_z / \varepsilon_n} \right) \tag{11}$$

where σ_z and ε_z are the longitudinal stress and strain of concrete, respectively; E_1 is the initial tangent modulus of concrete; E_2 is the slope of the asymptotic line of the second part of the stress-strain curve (refer to Fig. 9b) after the turning point; f_o is the vertical coordinate of the intersection between the asymptotic line and y -axis; n is the curve-shape parameter that governs the curvature of the transition zone; and $\varepsilon_n = n \varepsilon_o$ in which $\varepsilon_o = f_o / E_1$. Wu and Jiang (2013) suggested using a constant value for the parameter n which was found to be insensitive to the overall stress-strain curve and thus could be determined from concentrically-loaded specimens. Values of $E_2/E_{2,0}$ and $f_o/f_{o,0}$, where $E_{2,0}$ and $f_{o,0}$ are values of the corresponding parameters when the load eccentricity is zero, are given by:

$$\frac{E_2}{E_{2,0}} = 1 + 5.55 \left(\frac{e}{R} \right)^{2.49} \left(\frac{E_f t_f}{E_1 R} \right)^{0.11} \tag{12}$$

$$\frac{f_o}{f_{o,0}} = 1 + 7.02 \left(\frac{e}{R} \right)^{1.67} \left(\frac{E_f t_f}{E_1 R} \right)^{0.32} \tag{13}$$

where R is the radius of column cross section.

On the other hand, Lin and Teng (2019) have just refined the Lam and Teng (2003) model to include both the ascending and descending types of stress-strain

curves encountered under eccentric loading. The model, given by Eq. 14, consists of a parabolic first segment and a linear second segment.

$$f_c = \begin{cases} E_c \varepsilon_c - \frac{(E_c - E_{2,ecc})^2}{4f'_c} \varepsilon_c^2 & 0 \leq \varepsilon_c < \varepsilon_t \\ f'_c + E_{2,ecc} \varepsilon_c & \varepsilon_t \leq \varepsilon_c \leq \varepsilon_{ccu,ecc} \end{cases} \quad (E_{2,ecc} \geq 0) \tag{14a}$$

$$f_c = \begin{cases} E_c \varepsilon_c - \frac{E_c^2}{4f'_c} \varepsilon_c^2 & 0 \leq \varepsilon_c < \varepsilon_t \\ f_t + E_{2,ecc} (\varepsilon_c - \varepsilon_t) & \varepsilon_t \leq \varepsilon_c \leq \varepsilon_{ccu,ecc} \end{cases} \quad (E_{2,ecc} < 0) \tag{14b}$$

where ε_t and f_t are the transition strain and stress between the two segments of the stress-strain curve and can be determined using Eqs. 15 and 16, respectively.

$$\varepsilon_t = \begin{cases} \frac{2f'_c}{E_c - E_{2,ecc}} & (E_{2,ecc} \geq 0) \\ \frac{2f'_c (E_c - E_{2,ecc})}{E_c^2} & (E_{2,ecc} < 0) \end{cases} \tag{15}$$

$$f_t = \begin{cases} f'_c + E_{2,ecc} \varepsilon_t & (E_{2,ecc} \geq 0) \\ E_c \varepsilon_t - \frac{E_c^2}{4f'_c} \varepsilon_t^2 & (E_{2,ecc} < 0) \end{cases} \tag{16}$$

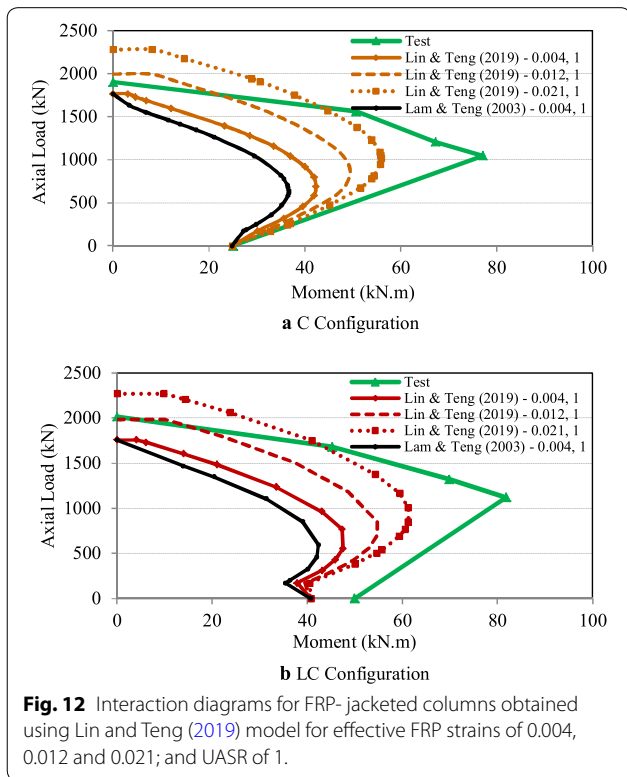
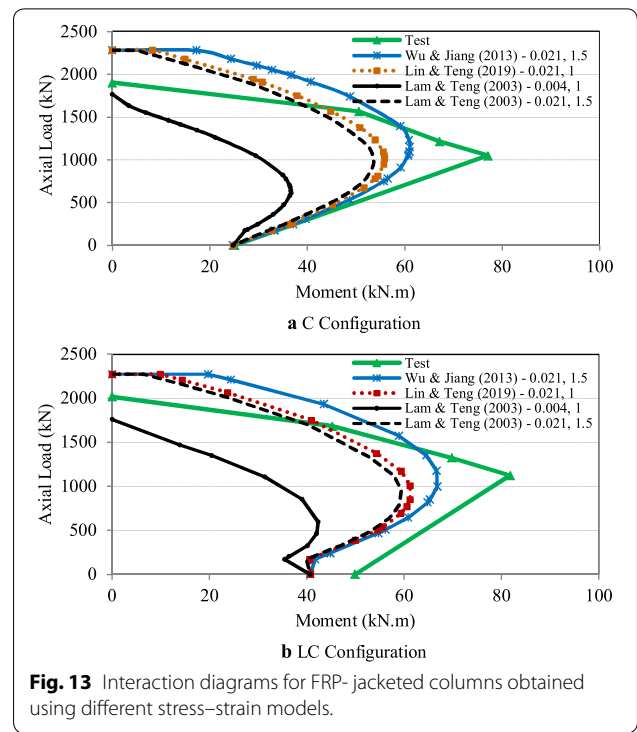
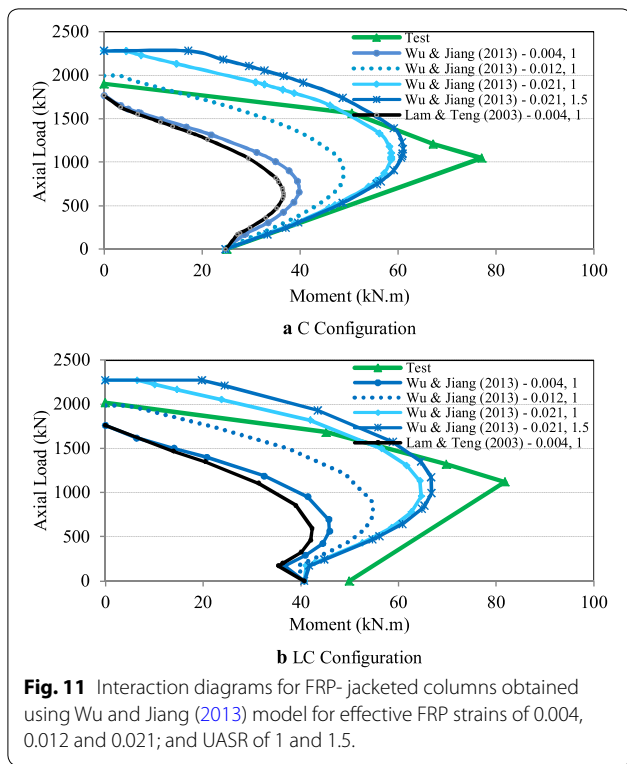
The second-segment slope ($E_{2,ecc}$) and the ultimate axial strain ($\varepsilon_{ccu,ecc}$) of the stress-strain model proposed by Lin and Teng (2019) depend on the total actual load eccentricity (represented by the diameter-to-compression depth ratio, i.e. D/c , where c is equal to the depth of the compression zone) and can be computed using the following equations

$$E_{2,ecc} = E_{2,con} \left(1 - 0.0808 \frac{E_{2,con}}{|E_{2,con}|} \frac{D}{c} \right), \quad \frac{D}{c} \leq 12.4 \tag{17}$$

$$\varepsilon_{ccu,ecc} = \varepsilon_{ccu,con} \left(1 + 0.263 \frac{D}{c} + 0.0227 \left(\frac{D}{c} \right)^2 \right) \tag{18}$$

One should note that Eq. 18 takes into account the increase in ultimate axial strains under eccentric loading as noted by Wu and Jiang (2013). However, Lin and Teng (2019) associated this increase with the level of load eccentricity via the D/c ratio rather than assuming a constant increase regardless of the eccentricity level as reported by Wu and Jiang (2013).

Figures 11 and 12 show the $P-M$ interactions predicted for the FRP-wrapped columns using the stress-strain models described by Eqs. 11 and 14, respectively. Three



values for the effective FRP strain were considered (0.004, 0.012 and 0.021) in these predictions. In both figures, the theoretical $P-M$ predictions are compared with the experimental curves as well as those obtained using the Lam and Teng (2003) stress-strain model and restrictions ($\epsilon_{fe} \leq 0.004$) of the ACI 440.2R-17 (2017) design guidelines. Inspection of the two figures reveals that even at an effective strain value of 0.004, the eccentricity-dependent models result in higher estimates, compared to those predicted using ACI 440.2R-17 (2017) guidance, of the moment resistance at a specific axial force. Further increases in moment resistance are obtained with the increase in effective FRP strains however this has been shown to overestimate the axial column resistance under small e/D ratios. A similar trend is also observed upon using an ultimate axial strain ratio of 1.5 between eccentric loading and concentric loading in the Wu and Jiang (2013) model.

To gain better insights into the effect of the stress-strain model on strength predictions; $P-M$ curves obtained using the three models (Wu and Jiang 2013; Lin and Teng 2019; Lam and Teng 2003) with an effective FRP strain of 0.021 and an ultimate axial strain ratio of 1.5 (as applicable) are shown in Fig. 13. Examination of Fig. 13 shows that the Lin and Teng (2019) model

predicts a similar trend to that obtained by the Lam and Teng (2003) model with an UASR value of 1.5. One can conclude that using the Lam and Teng (2003) model which was originally proposed for concentrically-loaded columns but with due consideration of the probable increase in ultimate axial strains under eccentric loading could reflect, roughly, the effects of load eccentricity on the stress–strain behavior of FRP-confined columns. This observation is only valid for the purpose of predicting P – M interactions using section analysis and is not intended for predictions of ultimate displacements/strains. Compared to the models developed by Teng and his colleagues (Lin and Teng 2019; Lam and Teng 2003), higher estimates of the axial strength under small e/D ratios and higher, yet conservative, estimates of the flexural strength under large e/D ratios were obtained via the Wu and Jiang (2013) model.

Results presented in this section call attention to the unsuitability of using a stress-model developed for FRP-confined concrete under concentric compression to predict the stress–strain behavior of the eccentrically-loaded columns even when the effect of the eccentricity-induced strain gradient is taken into account. This research questions the appropriateness of design models adopted by international guidelines for FRP-confined concrete under eccentric loading and the use of FRP-confined stress–strain models that have been based on and calibrated to fit a limited set of experimental results. In summary, the numerical analyses presented in this study have substantiated the need to revise the design approach suggested by ACI 440.2R-17 (2017). The authors believe that an eccentricity-dependent stress–strain model should be used for columns under eccentric loading when the eccentricity-to-diameter ratio exceeds 0.1 and suggest using an ultimate axial strain ratio of 1.5 between a column under eccentric loading and the corresponding column under concentric loading. In addition to published literature, further investigations into the behavior of eccentrically-loaded RC columns are still needed to build a comprehensive database on the effects of a wide spectrum of load eccentricities on the stress–strain relation of FRP-confined concrete sections.

5 Conclusions

Based on the test results of 25 medium-scale circular RC columns under axial–flexural interaction and the numerical analysis conducted in this study, the following main conclusions are drawn:

1. Reductions in axial resistance with the increase in load eccentricity were found to be less pronounced in FRP-wrapped columns than in unwrapped columns. Whilst reductions of about 35% and 44% were noted

in axial resistance of FRP-jacketed specimens as e/D ratios reached 0.26 and 0.34, respectively; higher reductions of about 42% and 49% were noted in their companion control specimens. To the contrary, higher reductions in ductility and toughness were noted in FRP-wrapped columns with the increase in load eccentricity. A 39% reduction in ductility of the control columns was reported as e/D increased to 0.26 whereas higher reductions of 58% and 63% were reported in their counterpart columns wrapped with the C and LC configurations, respectively.

2. Hoop FRP confinement can be efficiently used to improve the strength (25–35%) and deformation capacity (34–124%) of eccentrically-loaded columns. However, beneficial effects of FRP confinement on axial deformation capacity, ductility and toughness were found to be inversely proportional to the loading eccentricity in compliance with the existing literature.
3. Compared to columns under pure compression, relative enhancement in ultimate column resistance provided by the hoop FRP wraps was found to be more significant at higher load eccentricities. The confinement-induced improvements in axial strength increased from 23% to about 35% as the loading eccentricity increased from 0 to 0.34 D .
4. Hoop FRP confinement allowed the eccentrically-loaded columns to attain higher lateral deformations reaching up to 5 times that of unconfined columns at load eccentricities within the compression failure zone and up to 2 or 3 times in the tension failure zone.
5. Using longitudinal FRP sheets as per the LC configuration resulted in substantial improvements in flexural column capacities that reached 52% under loading eccentricities of 0.34 D . Compared to unwrapped specimens, the LC jacketing system provided considerable increases (up to 115%) in the flexural resistance of specimens tested in pure bending. This finding confirms existing research results.
6. The 2-ply FRP wrapping system investigated in this study enabled the eccentrically-loaded columns to sustain higher ultimate axial displacements (1.5–2 times) combined with a general increase in lateral deformability and significant enhancements in ductility (1.3–1.6 times) and toughness (2–4 times) compared to their companion control columns.
7. Whilst the use of the 2-ply FRP jacket resulted in minor enhancements in axial resistance of eccentrically-loaded columns compared to their hoop FRP-confined companions that did not exceed 9%, this enhancement was found to be nearly constant regardless of the increase in loading eccentricity and

was accompanied by substantial reductions (49–74%) in lateral deflections for columns subjected to load eccentricities less than $0.26D$.

8. Using the stress–strain model of FRP-confined concrete adopted by ACI 440.2R-17 (2017), which was derived from test results of plain concrete cylinders of limited height-to-diameter ratios under concentric compression, overestimated the axial resistance of the concentrically-loaded FRP-confined columns by about 5%. However, the use of conventional section analysis in conjunction with the same stress–strain model and the limitations imposed on the effective FRP strain at failure in confined columns under eccentricities exceeding $0.1D$ underestimated the moment resistance of FRP-jacketed columns under a certain axial force over the full range of load eccentricities used in the experimental program.
9. Better predictions of P – M interactions in the eccentrically-loaded FRP-confined columns were obtained by using eccentricity-dependent stress–strain models when the load eccentricity exceeded $0.1D$. Using the Lam and Teng (2003) stress–strain model resulted in similar predictions when considering the increase in ultimate axial strains of FRP-confined concrete sections under eccentric loading. An ultimate strain ratio of 1.5 between an eccentric loaded column and the corresponding concentric loaded column could be used regardless of the eccentricity-to-diameter ratio.

Acknowledgements

Experimental work presented in this article was funded by the Deanship of Research at Jordan University of Science and Technology under Grant No. 2016/381.

Authors' contributions

HA supervised the experimental program and participated in data collection and analysis. RA designed and conducted the experimental program and participated in data collection and analysis. HA wrote the manuscript. Both authors read and approved the final manuscript.

Funding

The experimental work presented in this article was funded by the Deanship of Research at Jordan University of Science and Technology under Grant No. 2016/381.

Role of the Funding Source: Deanship of Scientific Research at Jordan University of Science and Technology funded the investigation subject of the paper. The sponsor had no role in the study design, in the collection, analysis and interpretation of data, in the writing of the report, and in the decision to submit the paper for publication.

Availability of data and materials

The datasets used and/or analyzed during the current study are available from the corresponding author on reasonable request.

Competing interests

The authors declare that they have no competing interests.

Received: 20 February 2019 Accepted: 14 August 2019
Published online: 28 October 2019

References

- ACI 211.1-91. (1991). Standard practice for selecting properties for normal, heavyweight and mass concrete (reapproved 2009). Farmington Hills, MI: American Concrete Institute.
- ACI 318-14. (2014). Building code requirements for structural concrete and commentary. Farmington Hills, MI: American Concrete Institute.
- ACI 440.2R-17. (2017). Guide for the design and construction of externally bonded FRP systems for strengthening concrete structures. Farmington Hills: American Concrete Institute.
- Al-Nimry, H., & Neqresh, M. (2019). Confinement effects of unidirectional CFRP sheets on axial and bending capacities of square RC columns. *Engineering Structures*. <https://doi.org/10.1016/j.engstruct.2019.109329>.
- Al-Nimry, H., & Soman, A. (2018). On the slenderness and FRP confinement of eccentrically-loaded circular RC columns. *Engineering Structures*, *164C*, 92–108.
- Bisby, L., & Ranger, M. (2010). Axial–flexural interaction in circular FRP-confined reinforced concrete columns. *Construction and Building Materials*, *24*(9), 1672–1681.
- Cao, Y.-G., Wu, Y.-F., & Jiang, C. (2018). Stress–strain relationship of FRP confined concrete columns under combined axial load and bending moment. *Composites Part B: Engineering*, *134*, 207–217.
- Chaallal, O., & Shahawy, M. (2000). Performance of fiber-reinforced polymer-wrapped reinforced concrete column under combined axial–flexural loading. *ACI Structural Journal*, *97*(4), 659–668.
- Chellapandian, M., & Prakash, S. S. (2019). Axial compression–flexure interaction behavior of hybrid FRP strengthened columns. *ACI Structural Journal*, *116*(2), 125–138. <https://doi.org/10.14359/51710877>.
- Chellapandian, M., Prakash, S. S., Mahadik, V., & Sharma, A. (2019a). Experimental and numerical studies on effectiveness of hybrid FRP strengthening on behavior of RC columns under high eccentric compression. *Journal of Bridge Engineering*. [https://doi.org/10.1061/\(ASCE\)BE.1943-5592.0001420](https://doi.org/10.1061/(ASCE)BE.1943-5592.0001420).
- Chellapandian, M., Prakash, S. S., & Sharma, A. (2019b). Experimental investigation of the effectiveness of hybrid FRP-strengthened RC columns on axial compression–bending interaction behavior. *Journal of Composites for Construction*, *23*(4), 04019025. [https://doi.org/10.1061/\(ASCE\)CC.1943-5614.0000952](https://doi.org/10.1061/(ASCE)CC.1943-5614.0000952).
- CNR. (2013). *CNR-DT 200 R1/2013: Guide for the design and construction of externally bonded FRP systems for strengthening existing structures*. Rome: Italian Research Council CNR Advisory Committee on Technical Recommendations for Construction.
- Csuka, B., & Kollár, L. (2012). Analysis of FRP confined columns under eccentric loading. *Composite Structures*, *94*(3), 1106–1116.
- Daugevičius, M., Valivonis, J., Beinavičius, A., Skuturna, T., & Budvytis, M. (2013). Experimental investigation of the load carrying capacity of eccentrically loaded reinforced concrete elements strengthened with CFRP. *Procedia Engineering*, *57*, 232–237.
- Di Nardo, A., Faella, C., & Realforzo, R. (2006). A design procedure of FRP confining systems for upgrade R/C columns. In *Proceedings of 3rd Int. Conf. on FRP Composites in Civil Engineering (CICE)*, Miami, USA, 13–15 December 2006.
- El Maaddawy, T. (2009). Strengthening of eccentrically loaded reinforced concrete columns with fiber-reinforced polymer wrapping system: Experimental investigation and analytical modeling. *Journal of Composites for Construction*, *13*(1), 13–24.
- El Maaddawy, T., El Sayed, M., & Abdel-Magid, B. (2010). The effects of cross-sectional shape and loading condition on performance of reinforced concrete members confined with carbon fiber-reinforced polymers. *Materials and Design*, *31*(5), 2330–2341.
- Fahmy, M., & Farghal, O. (2016). Eccentricity-based design-oriented model of fiber-reinforced polymer-confined concrete for evaluation of load-carrying capacity of reinforced concrete rectangular columns. *Journal of Reinforced Plastics and Composites*, *35*(23), 1734–1758.
- Fitzwilliam, J., & Bisby, L. (2010). Slenderness effects on circular CFRP confined reinforced concrete columns. *Journal of Composites for Construction*, *14*(3), 280–288.

- Ghali, K., Rizkalla, S., Kassem, M., Fawzy, T., & Mahmoud, M. (2003). FRP-confined circular columns under small eccentric loading. In *Proceedings of 5th Alexandria Int. Conf. on Structural and Geotechnical Engineering, Alexandria University, Egypt, 20–27 December 2003*.
- Hadi, M. (2006a). Behavior of FRP wrapped normal strength concrete columns under eccentric loading. *Composite Structures*, 72(4), 503–511.
- Hadi, M. (2006b). Comparative study of eccentrically loaded FRP wrapped columns. *Composite Structures*, 74(4), 127–135.
- Hadi, M. (2007). Behaviour of FRP strengthened concrete columns under eccentric compression loading. *Composite Structures*, 77(1), 92–96.
- Hadi, M. (2009). Behaviour of eccentric loading of FRP confined fibre steel reinforced concrete columns. *Construction and Building Materials*, 23(2), 1102–1108.
- Hadi, M., & Widiarsa, I. (2012). Axial and flexural performance of square RC columns wrapped with CFRP under eccentric loading. *Journal of Composites for Construction*, 16(6), 640–649.
- Lam, L., & Teng, J. (2003). Design-oriented stress–strain model for FRP-confined concrete. *Construction and Building Materials*, 17(6–7), 471–489.
- Li, J., & Hadi, M. (2003). Behavior of externally confined high-strength concrete columns under eccentric loading. *Composite Structures*, 62, 145–153.
- Lin, G., & Teng, J.G. (2016). Stress–strain behaviour of FRP-confined concrete in eccentrically-loaded circular columns. In *Proceedings of 8th Int. Conf. on Fibre-Reinforced Polymer (FRP) Composites in Civil Engineering (CICE 2016) Hong Kong, China*.
- Lin, G., & Teng, J. G. (2017). Three-dimensional finite-element analysis of FRP-confined circular concrete columns under eccentric loading. *Journal of Composites for Construction*, 21(4), 04017003. [https://doi.org/10.1061/\(ASCE\)CC.1943-5614.0000772](https://doi.org/10.1061/(ASCE)CC.1943-5614.0000772).
- Lin, G., & Teng, J. G. (2019). Stress–strain model for FRP-confined concrete in eccentrically loaded circular columns. *Journal of Composites for Construction*. [https://doi.org/10.1061/\(ASCE\)CC.1943-5614.0000946](https://doi.org/10.1061/(ASCE)CC.1943-5614.0000946).
- Nanni, A., & Norris, M. (1995). FRP jacketed concrete under flexure and combined flexure–compression. *Construction and Building Materials*, 9(5), 273–281.
- Parvin, A., & Wang, W. (2001). Behavior of FRP jacketed concrete columns under eccentric loading. *Journal of Composites for Construction*, 5(3), 146–152.
- Pham, T. M., Doan, L. V., & Hadi, M. N. (2013). Strengthening square reinforced concrete columns by circularisation and FRP confinement. *Construction and Building Materials*, 49, 490–499.
- Popovics, S. (1973). A numerical approach to the complete stress–strain curve of concrete. *Cement and Concrete Research*, 3, 583–599.
- Rocca, S., Galati, N., & Nanni, A. (2009). Interaction diagram methodology for design of FRP-confined reinforced concrete columns. *Construction and Building Materials*, 23(4), 1508–1520.
- Sadeghian, P., Rahai, A., & Ehsani, M. (2010). Experimental study of rectangular RC columns strengthened with CFRP composites under eccentric loading. *Journal of Composites for Construction*, 14(4), 443–450.
- Song, X., Gu, X., Li, Y., Chen, T., & Zhang, W. (2013). Mechanical behavior of FRP-strengthened concrete columns subjected to concentric and eccentric compression loading. *Journal of Composites for Construction*, 17(3), 336–346.
- Tao, Z., Teng, J.G., Han, L.-H., & Lam, L. (2004). Experimental behaviour of FRP-confined slender RC columns under eccentric loading. In *Proceedings of 2nd Int. Conf. on Advanced Polymer Composites for Structural Applications in Construction, University of Surrey, UK, 20–22 April 2004*.
- TR 55. (2012). Design guidance for strengthening concrete structures using fibre composite materials (3rd ed.). Technical Report No. 55, Crowthorne, UK: Concrete Society.
- Vuggumudi, S., & Alagusundaramoorthy, P. (2018). Interaction diagrams for FRP strengthened RC rectangular columns with large aspect ratio. *Construction and Building Materials*, 171, 187–196. <https://doi.org/10.1016/j.conbuildmat.2018.03.131>.
- Widiarsa, I., & Hadi, M. (2013). Performance of CFRP wrapped square reinforced concrete columns subjected to eccentric loading. *Procedia Engineering*, 54, 365–376.
- Wu, Y.-F., & Cao, Y.-G. (2017). Effect of load path on behavior of FRP-confined concrete. *Journal of Composites for Construction*. [https://doi.org/10.1061/\(ASCE\)CC.1943-5614.0000799](https://doi.org/10.1061/(ASCE)CC.1943-5614.0000799).
- Wu, Y.-F., & Jiang, C. (2013). Effect of load eccentricity on the stress–strain relationship of FRP-confined concrete columns. *Composite Structures*, 98, 228–241.
- Yang, J., Wang, J., & Wang, Z. (2018). Rectangular high-strength concrete columns confined with carbon fiber-reinforced polymer (CFRP) under eccentric compression loading. *Construction and Building Materials*, 193, 604–622.
- Yi, W.-J., Xian, Q.-I., Ding, H.-T., & Zhang, H.-Y. (2006). Experimental study of RC columns strengthened with CFRP sheets under eccentric compression. *ACI Special Publication*, 238, 395–410.
- Youcef, Y., Amziane, S., & Chemrouk, M. (2015). CFRP confinement effectiveness on the behavior of reinforced concrete columns with respect to buckling instability. *Construction and Building Materials*, 81, 81–92.

Publisher's Note

Springer Nature remains neutral with regard to jurisdictional claims in published maps and institutional affiliations.

Submit your manuscript to a SpringerOpen[®] journal and benefit from:

- Convenient online submission
- Rigorous peer review
- Open access: articles freely available online
- High visibility within the field
- Retaining the copyright to your article

Submit your next manuscript at ► [springeropen.com](https://www.springeropen.com)